ELECTRONIC PROPERTIES OF NON-CIRCULAR QUANTUM DOTS

Esa Räsänen

Laboratory of Physics
Helsinki University of Technology
Espoo, Finland

Dissertation for the degree of Doctor of Science in Technology to be presented with due permission of the Department of Engineering Physics and Mathematics for public examination and debate in Auditorium K at Helsinki University of Technology (Espoo, Finland) on the 28th of May, 2004, at 12 o'clock noon.

Dissertations of Laboratory of Physics, Helsinki University of Technology
ISSN 1455-1802

Dissertation 128 (2004):
Esa Räsänen: Electronic properties of non-circular quantum dots
ISBN 951-22-7100-1 (print)
ISBN 951-22-7101-X (electronic)

Otamedia OY
ESPOO 2004

Abstract

Quantum dots are nanoscale electronic objects, typically fabricated using two-dimensional semiconductor heterostructures or three-dimensional atomic clusters. In addition to promising technological applications, quantum dots represent excellent sources of interesting many-electron quantum physics.

This thesis deals with the theoretical modeling of two-dimensional quantum dots consisting of less than twenty electrons. The aim is to clarify how the geometry of the confining potential affects the ground-state structure of the system with and without the presence of an external magnetic field. The question is of a great importance in understanding and predicting the basic electronic properties of actual quantum-dot devices.

The calculations are based on the density-functional theory applied within a real-space multigrid approach, which is shown to be a powerful method for the systems considered in this thesis. The accuracy of the method is, however, highly dependent on the local spin-density approximation used. Hence, different parametrizations for the exchange-correlation energy are compared. Furthermore, the problem of the density-functional theory as a mean-field approach using a single-configuration wave function is analyzed in this thesis.

Quantum dots of various shapes are investigated, beginning with polygonal systems to determine the critical densities for the Wigner crystallization. Rectangular dots are shown to be particularly sensitive to the geometry, but a qualitative agreement is obtained with the experimental addition energy spectra. The lack of circular symmetry does not prevent the maximum-density-droplet formation when an external magnetic field is applied, and the high-field limit may be characterized by remarkably regular state oscillations. The symmetry can also be distorted by an external impurity, for which a realistic model is obtained with a comparison to experimental data. Presumably, some of the rich variety of phenomena identified in this thesis for non-circular quantum dots will have a realization in the future nanoelectronics.

Preface

This thesis has been prepared in the Computational Condensed Matter and Complex Materials Group in the Laboratory of Physics at the Helsinki University of Technology during the years 2002-2004.

I am grateful to Academy Prof. Risto Nieminen for the dynamic management of this group and for the scientific contribution and advice. I wish to express my gratitude to my supervisor, Prof. Martti Puska for the introduction to this inspiring field and for the excellent guidance throughout this work.

I am indebted to Henri Saarikoski, whose contribution especially in developing the computational programs has been essential for these studies, and to Ari Harju for enlightening me on several physical concepts related to the theory and the methods. I am glad to thank Prof. Rolf Haug and Jens Könemann at the University of Hannover for the successful collaboration and for their hospitality during my visit. I am also grateful to Sami Siljamäki, the rest of the Nabel group, Tuomas Torsti, Karri Niemelä, and Prof. Juhani von Boehm for the contribution and the useful discussions.

Generally, I wish to thank the whole personnel of the Laboratory of Physics for the nice working atmosphere, particularly my office mates Miguel Gosálvez and Ville Vuorinen. I also thank my family, all my friends, and especially Johanna for the support during this work.

The financial support from the Academy of Finland, the Magnus Ehrnrooth Foundation, the Väisälä Foundation, and the Emil Aaltonen foundation is gratefully acknowledged.

Helsinki, February 2004

Esa Räsänen

Contents

List of publications

This thesis consists of an overview and the following publications:

I E. Räsänen, H. Saarikoski, M. J. Puska, and R. M. Nieminen, *Wigner molecules in polygonal quantum dots: A density-functional study*, Physical Review B **67**, 035326 (2003).

II E. Räsänen, H. Saarikoski, V. N. Stavrou, A. Harju, M. J. Puska, and R. M. Nieminen, *Electronic structure of rectangular quantum dots*, Physical Review B **67**, 235307 (2003).

III H. Saarikoski, E. Räsänen, S. Siljamäki, A. Harju, M. J. Puska, and R. M. Nieminen, *Testing of two-dimensional local approximations in the current-spin and spin-density-functional theories*, Physical Review B **67**, 205327 (2003).

IV A. Harju, E. Räsänen, H. Saarikoski, M. J. Puska, R. M. Nieminen, and K. Niemelä, *Broken symmetry in density-functional theory: Analysis and cure*, Physical Review B **69**, 153101 (2004).

V E. Räsänen, M. J. Puska, and R. M. Nieminen, *Maximum-density-droplet formation in hard-wall quantum dots*, Physica E **22**, 490 (2004).

VI E. Räsänen, A. Harju, M. J. Puska, and R. M. Nieminen, *Rectangular quantum dots in high magnetic fields*, Physical Review B **69**, 165309 (2004).

VII E. Räsänen, J. Könemann, R. J. Haug, M. J. Puska, and R. M. Nieminen, *Impurity effects in quantum dots: Towards quantitative modeling*, submitted to Physical Review B.

The author has had an active role in all the phases of the research reported in this thesis. He has contributed to the development of the computer program employed to calculate the results presented in Publications I, II, and IV-VII. The author has designed the work and performed the calculations reported in Publications I, II, and V-VII, and has written the main drafts of those papers. He has contributed to the computation of the results and the writing process of Publications III and IV.

Chapter 1

Introduction

In the rapidly expanding field of nanotechnology, semiconductor quantum dots represent basic elements of novel nanoelectronic components. They have dimensions from nanometers to a few microns and contain a controlled number of electrons, typically from one to several thousands. The tunable shape, size, and electron number of these "artificial atoms", as well as their pronounced electron-electron correlation effects, make them excellent objects for studying various many-electron phenomena. From the numerous eventual applications of these objects, including quantum-dot lasers and single-electron transistors, the most intriguing are quantum bits (qubits) that might be used in quantum computing in the future.

Electrons in quantum dots are usually confined in an interface of a semiconductor heterostructure, e.g. GaAs/AlGaAs, so that the transverse dimensions, controlled by a lateral confinement, are considerably larger than the thickness of the dot. In modeling quantum dots, the most common approximation for the flat disk-like shape is a two-dimensional well with a parabolic confinement potential. In most cases this model describes the movement of the electrons with a reasonable accuracy. The variety of different quantum-dot shapes is, however, continuously extending due to the rapid development of fabrication methods. The modeling of new nanoelectronic devices sets great demands on the computational tools, since the deviation from a circular geometry generally makes the many-electron problem particularly complicated to solve, especially in the presence of a magnetic field.

The objective of this thesis is to clarify the ground-state electronic properties of quantum dots where the confining potential is not of the standard parabolic shape, but polygonal, rectangular, or contains an external impurity. The emphasis is laid on determining the effects of electron-electron interactions and the external

magnetic field on the energies, electron densities, chemical potentials, spin evolution, magnetization, and total angular momentum. In addition, single-electron properties are considered in order to estimate the importance of the interactions, and also to visualize the underlying chaotic properties that arise from the nonintegrability of the corresponding eigenvalue equation in the presence of a magnetic field.

The results presented in this thesis have been obtained by using the spin-density-functional theory and the effective-mass approximation for electrons in GaAs. As a mean-field theory, the density-functional approach reduces the complicated many-body problem to a model of independent electrons moving in an effective potential that includes all the mutual interactions. The electron density and the total energy are then solved efficiently from the self-consistent Kohn-Sham equations. The calculations are performed in a real-space grid, which gives the advantage to shape the external potential arbitrarily. This feature is essential when modeling the systems of the present work.

Another aim in this thesis is to discuss two critical points of the density-functional methods. First, different parametrizations for the local spin-density approximations are compared in order to find the most accurate estimate for the exchange-correlation energy. Second, the formation of solutions with a broken spin symmetry in rectangular quantum dots is clarified with the help of exact diagonalization calculations. It is shown that a mean-field method using a single-configuration wave function can lead to a wrong mixing of different spin states.

The scope of this thesis is thus twofold: modeling of various two-dimensional quantum-dot systems and methodical analysis of the density-functional approach. The main contribution is a novel treatment of interacting electrons in non-circular quantum dots which, for many present computational methods, have been limited to only a few electrons in zero magnetic field. However, the results are compared with those of quantum Monte Carlo simulations, exact diagonalization, and other density-functional calculations whenever possible. Furthermore, the addition energy spectra of rectangular quantum dots and the single-electron spectrum of an impurity-containing dot are compared to experiments.

The organization of this thesis is as follows. In Chapter 2 the concept of a semiconductor quantum dot is presented on the basis of both experiments and theory, including a brief review of the current research on the topic. Chapter 3 deals with the density-functional theory, beginning from the basic principles, and continuing with the local spin-density approximations which are compared in detail in Publication III. Finally, the problem of broken spin-symmetries is presented as a summary of Publication IV. Chapter 4 introduces the numerical method applied in this thesis, i.e., the real-space multigrid technique. In Chapter 5 the main results for non-circular quantum dots are briefly presented. The first subjects

are the Wigner crystallization in polygonal quantum dots and the basic properties of rectangular quantum dots studied in Publications I and II, respectively. Thereafter, the effects of the magnetic field on these systems are presented. First, the chaotic properties in the single-electron spectra are discussed (unpublished), and then the results for the maximum-density droplet as well as for the high-field states are summarized in the connection with Publications V and VI. Finally, the effects induced by external impurities are discussed, referring to Publication VII. A summary of the complete thesis is presented in Chapter 6.

Chapter 2

Concept of a quantum dot

2.1 Fabrication

Semiconductor quantum dots are fabricated with several different methods [1]. The common objective between the techniques is to produce a lateral confinement of the two-dimensional electron gas (2DEG) at the interface between two semiconducting materials. One of the earliest methods was to create metal electrodes on the heterostructure surface with lithographic techniques [see Fig. 2.1(a)]. A voltage applied to the electrodes confines the 2DEG existing at the interface between the layers of different materials, e.g., GaAs and AlGaAs, into a small area. The density of the 2DEG can be controlled by the gate voltage applied to the conductive substrate [2]. The benefit of the method is the absence of edge defects, characteristic of etched quantum dots. A serial structure of lateral quantum dots may also be suitable for quantum computation, since all the tunnel barriers can be freely controlled [3]. This would require the isolation of a single electron, which was recently achieved for a lateral quantum-dot structure by Elzerman *et al.* [4]

Reed and co-workers [5] performed the pioneering experiments in creating vertical quantum-dot systems by etching techniques. By inserting electric contacts on the both ends of the heterostructure pillars and measuring electronic transport through the device, they could observe a discrete spectrum of quantum states. Later, Tarucha *et al.* [6] managed to measure Coulomb oscillations in vertical quantum dots containing a controlled number of electrons, and a clear shell structure was revealed. A schematic diagram of the double-barrier heterostructure and a picture of the sample are shown in Fig. 2.1(b). The dot is formed between nonconducting barrier layers, separating it from the source and drain contacts, and the lateral potential is tuned by a negative voltage applied to a metal gate around

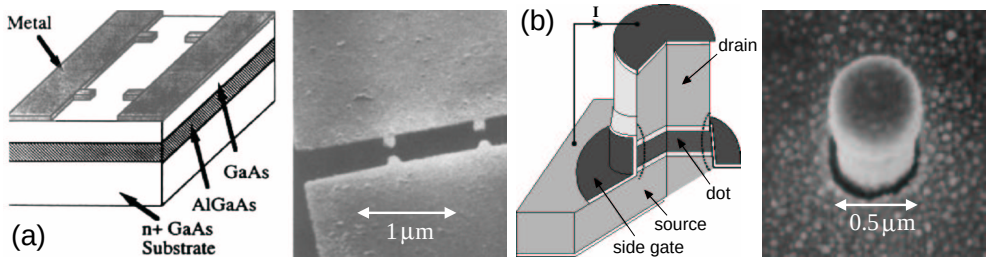

Figure 2.1: Schematic diagrams and scanning electron micrographs of lateral (a) (from Ref. [2]) and vertical (b) (from Ref. [7]) semiconductor quantum-dot devices.

the pillar. In comparison with lateral quantum dots, the number of electrons is generally easier to control in the vertical transport. Since etching techniques also enable the shaping of the quantum-dot geometry, the systems considered in this thesis can be more likely associated with vertical than lateral quantum dots.

Quantum dots can also be fabricated using a growth mechanism of a semiconducting compound on the surface of a material with a wider band gap than the growing material. The growth can be selective or self-assembled, depending on the material parameters. In the latter case, a sufficient difference in the lattice constants between the compounds, e.g. GaAs and InAs, is required to induce the growth of quantum-dot structures. Self-assembled quantum dots are considerably smaller and more strongly confined than their lithographically fabricated counterparts. Hence, their energy-quantization regime is suitable for developing optical devices, e.g., quantum-dot lasers [8].

2.2 Experiments

Experiments on quantum dots have been mainly focused on electron transport properties and optical properties. Characteristic of the electron transport through the quantum dot is the Coulomb blockade: As the bias voltage is increased, an electron can pass through the dot when the energy in the system reaches the Coulomb energy $e^2/2C$. The current has therefore a stepwise increase, leading to the Coulomb staircase as a function of the bias voltage. If the bias voltage is kept below the Coulomb gap and the gate voltage is increased, the energy difference between the initial (no electrons) and final (one electron) state decreases. At the crossing point, corresponding to the maximum slope in the Coulomb staircase, electrons can tunnel into and out of the dot. The sequence of current peaks as a function of the gate voltage is shown in Fig. 2.2. The gaps are proportional to the addition energies that equal to the differences in the electrochemical potentials, $E_{\mathrm{add}} = \mu(N+1) - \mu(N) = E(N+1) - 2E(N) + E(N-1)$. In the

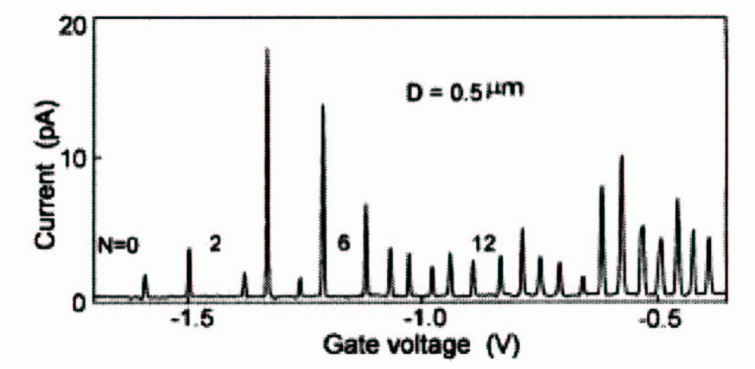

Figure 2.2: Coulomb blockade oscillations as a function of the gate voltage in a vertical quantum dot by Tarucha *et al.* [6]

qualitative constant-capacitance model, the addition energy is approximated as a sum of the (constant) Coulomb interaction and the energy difference between the single-electron energies, i.e., $E_{\text{add}} \approx e^2/C + \Delta\epsilon$. The peak spacings thereby offer information of the shell structure in the system, as mentioned above in context of vertical quantum dots [6]. Other techniques to investigate the single-electron charging effects are, for example, the gated transport spectroscopy and the single-electron capacitance spectroscopy reviewed by Ashoori in Ref. [9].

The optical properties of quantum dots are mainly related to the absorption or emission of light in the far-infrared (FIR) range, corresponding to the typical excitation energies in semiconductor quantum dots. Due to the relatively large wavelength of the FIR radiation, it couples only to the center-of-mass motion of the electrons [1]. The FIR spectroscopy is insensitive to the electron-electron interactions in the case of a quadratic potential, since in that case the relative and the center-of-mass motions can be separated in the Hamiltonian [10]. If the symmetry is lowered, these components of motion couple, allowing the study of interaction effects. Although this has motivated theoretical research of non-circular quantum dots [11–14], excitation effects are not studied in this thesis.

2.3 Single-electron spectra

The modeling of semiconductor quantum dots usually requires the effective-mass approximation (EMA), in which the electrons are given an effective mass m^*, equivalent to that of the conduction band electrons in the semiconductor material. The mutual interaction of the electrons is screened by the dielectric constant ϵ. For GaAs, the values are $m^* = 0.067\, m_e$ and $\epsilon = 12.4 \ldots 13$. The neutralizing

positive background charge present in real systems is usually taken into account through the external confinement potential.

The spinless single-electron (no electron-electron interactions) Hamiltonian for a two-dimensional quantum dot in the presence of a magnetic field and within the EMA can be written in SI units as

$$H_0 = \frac{1}{2m^*}\left(\mathbf{p} + e\mathbf{A}\right)^2 + V_{\text{ext}}(\mathbf{r}), \tag{2.1}$$

where the vector potential is chosen in the symmetric gauge, i.e., $\mathbf{A} = \frac{B}{2}(-y, x, 0)$, giving $\mathbf{B} = \nabla \times \mathbf{A} = B\hat{z}$ for the magnetic field. The external confining potential V_{ext} determines the geometry of dot and the (analytical) solvability of the single-electron eigenvalue equation,

$$H_0\psi_i = \epsilon_i\psi_i. \tag{2.2}$$

A standard approximation for the external confinement is a parabolic potential [15], i.e., $V_{\text{ext}}(r) = \frac{1}{2}m^*\omega_0^2 r^2$, where $\hbar\omega_0$ defines the confinement strength. This has proven an appropriate estimate in conventional quantum dots where the lateral confinement is created by metallic gates above the quantum well [16]. Detailed modifications to the parabolic approximation in lateral dots have been theoretically considered by Stopa [17]. Now the Hamiltonian (2.1) becomes

$$H_0 = \frac{p^2}{2m^*} + \frac{1}{2}m^*\left(\omega_0^2 + \frac{1}{4}\omega_c^2\right)r^2 + \frac{1}{2}\omega_c l_z, \tag{2.3}$$

where $\omega_c = eB/m^*$ is the cyclotron frequency, and $l_z = xp_y - yp_x$ is the z component of the angular momentum operator. The analytical solutions of Eq. (2.2) are the Fock-Darwin (FD) states [18] with the eigenenergies

$$\epsilon_{n,l} = (2n + |l| + 1)\hbar(\omega_0^2 + \frac{1}{4}\omega_c^2)^{1/2} - \frac{1}{2}l\hbar\omega_c, \tag{2.4}$$

where $n = 0, 1, 2, ...$ is the radial and $l = 0, \pm1, \pm2, ...$ is the azimuthal quantum number. Figure 2.3(a) shows the corresponding energy spectrum as a function of the magnetic field strength when $\hbar\omega_0 = 5$ meV and $2n + |l| \leq 6$. At $B = 0$ T, the system is a two-dimensional harmonic oscillator and when B increases, the eigenenergies degenerate into the ideal two-dimensional Landau levels corresponding to the limit $\hbar\omega_0 \to 0$.

A circular hard-wall quantum dot represents an another example of an analytically solvable model. It is defined by a simple well-like confining potential

$$V_{\text{ext}}(r) = \begin{cases} 0, & r \leq R \\ \infty, & r > R, \end{cases} \tag{2.5}$$

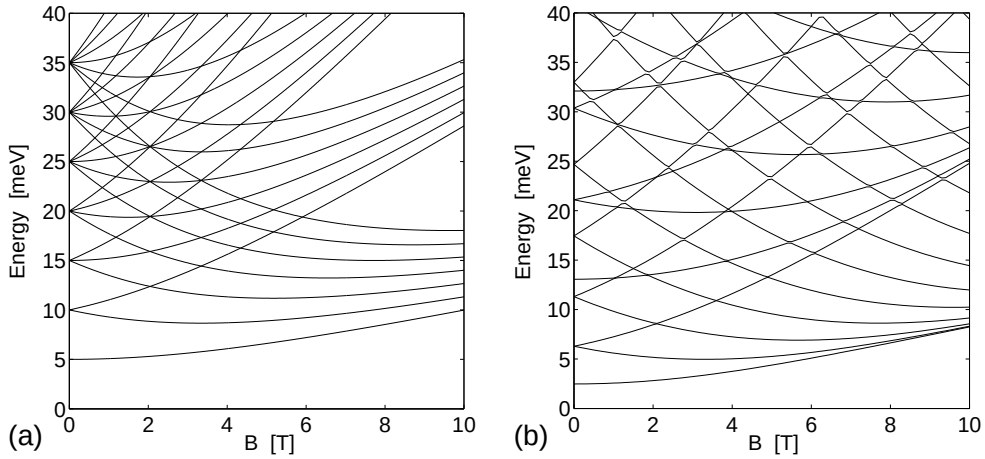

Figure 2.3: Lowest single-electron eigenenergies for a parabolic [(a), $\hbar\omega_0 = 5$ meV, $2n + |l| \leq 6$] and circular hard-wall [(b), $R \sim 36$ nm] quantum dot.

where R is the dot radius. Similarly to the parabolic case, the wave function is separable into radial and azimuthal parts due to the circular symmetry, and the single-electron eigenvalues are given by

$$\epsilon_{n,l} = \hbar\,\omega_c \left(\alpha_{nl} + \frac{l + |l|}{2} + \frac{1}{2} \right), \tag{2.6}$$

where α_{nl} are the zeroes of the confluent hypergeometric function. The energy spectrum in Fig. 2.3(b) is generally more complicated than the parabolic one at low magnetic fields. Geerinckx *et al.* [19] have found large differences in the optical properties between these systems.

Vertical quantum dots fabricated by etching techniques (see Sec. 2.1) have been expected to provide more well-defined confinement walls than lithographic systems [19], i.e., steeper edges for the dot than given by the parabolic approximation. However, no direct experimental signature of hard-wall potentials have yet been detected in vertical devices. Meanwhile, Fuhrer *et al.* [20] have shown that quantum dots fabricated by local oxidation with an atomic force microscope can be described by a steep-wall confinement.

If the symmetries in the confining potential in Eq. (2.1) cannot be adequately exploited, an analytical solution for the eigenvalue equation (2.2) may be obtained only in zero magnetic field. Then, exact eigenenergies can be considered, e.g., as a function of the deformation of the dot, as demonstrated for rectangular quantum dots in Publication III. The magnetic-field evolution of the eigenenergies can then be resolved with numerical methods, for example, with the exact diagonalization of the Hamiltonian. The energy spectrum of an analytically non-solvable system is

considerably different from, e.g., Figs. 2.3(a) and (b). Typically there are several avoided crossings between the energy levels. This refers to chaotic properties in the system, discussed in more detail in Sec. 5.3.1.

2.4 Many-electron problem

The corresponding many-body Hamiltonian for N electrons is written as

$$H = \frac{1}{2m^*}\sum_{i=1}^{N}\left[\mathbf{p}_i + e\mathbf{A}(\mathbf{r}_i)\right]^2 + \sum_{i<j}^{N}\frac{e^2}{4\pi\epsilon_0\epsilon|\mathbf{r}_i - \mathbf{r}_j|} + \sum_{i=1}^{N}\left[V_{\text{ext}}(\mathbf{r}_i) + g^*\mu_B B s_{z,i}\right], \quad (2.7)$$

where the mutual Coulomb interaction is now included, and the last term is the Zeeman energy that couples the external magnetic field with the electron spin. Here g^* is the effective gyromagnetic ratio for GaAs (typically -0.44), μ_B is the Bohr magneton, and $s_z = \pm\frac{1}{2}$ for the electron spin $\sigma = \uparrow, \downarrow$, respectively. The spin-orbit interaction [21] is excluded in the Hamiltonian, since it is supposed to be relatively small in a wide-gap material like GaAs unless $N \gtrsim 20$.

The direct solving of the many-body Schrödinger equation, $H\Psi = E\Psi$, is practically hopeless due to the huge amount of information stored in the many-body wave function, $\Psi = \Psi(\mathbf{r}_1^\sigma, \mathbf{r}_2^\sigma, \ldots, \mathbf{r}_N^\sigma)$. A feasible approach is to restrict the Hilbert space to a finite basis in which the Schrödinger equation is solved. This exact diagonalization (ED) or configuration-interaction method is, however, applicable to only a few electrons and high electron densities. Recently, a detailed ED study has been carried out for parabolic quantum dots in a magnetic field with three [22] and four electrons [23]. In strong magnetic fields the method is suitable up to around ten electrons, since the basis can be effectively restricted to consist of compatible states with the desired total angular momentum [24].

Quantum Monte Carlo (QMC) methods represent a statistical approach to the many-electron problem, providing integrated expectation values for the quantum mechanical observables. In the variational quantum Monte Carlo method (VMC), for example, the variational principle is applied to the trial wave functions in order to find the lowest possible upper bound of the true total energy. The expectation values are then computed as statistical averages of local quantities over the many-electron coordinate space. QMC methods have proven reliable tools in the study of quantum-dot systems up to a large number of electrons, and they give accurate results even at very low densities [25, 26].

Hartree-Fock (HF) approximations are based on writing the many-electron wave function as a Slater determinant satisfying the desired antisymmetric property of the fermionic wave functions. The exchange term is added explicitly, but the

correlation effects are not taken into account. Still, the HF approach is often an adequate approximation as far as the problems related to broken-symmetry solutions are properly taken into account. A detailed analysis of such solutions was recently performed by Reusch and Grabert [27] who used the unrestricted (orbital angular momenta not fixed) Hartree-Fock (UHF) method for parabolic quantum dots. Trail and co-workers [28] have studied the ability of the UHF to treat Wigner crystallization (see Sec. 5.1) in the 2DEG and 3DEG. The HF approximation is fundamentally based on the mean-field approach that describes independent electrons in an effective potential. In this respect it is reminiscent of the density-functional theory which is discussed in the next Chapter.

Chapter 3

Density-functional theory

The density-functional theory (DFT) has been one of the most successful methods in electronic structure calculations since it was formulated in the early 1960s. The main idea is to take the particle density instead of the many-body wave function as the basic variable to describe the ground state. The huge reduction in the degrees of freedom makes the DFT a powerful tool to study large systems with a moderate computational effort. It is formally an exact theory, but in actual calculations its accuracy depends on approximations as shown below.

3.1 Basic principles

The nonrelativistic time-independent Hamiltonian for a confined system of interacting electrons can be written as a sum of the kinetic, mutual Coulomb interaction, and external confinement operators,

$$\hat{H} = \hat{T} + \hat{V}_{\rm ee} + \hat{V}_{\rm ext}. \tag{3.1}$$

According to the Hohenberg-Kohn (HK) theorem [29], there is a one-to-one correspondence between the (nondegenerate) ground-state electron density $n(\mathbf{r})$ and the external potential $V_{\rm ext}(\mathbf{r})$ (within an additive constant). This can be easily proven using the variational principle. Since $V_{\rm ext}(\mathbf{r})$ fixes the Hamiltonian, $n(\mathbf{r})$ determines implicitly all the properties derivable from $\hat{H}$, i.e., the ground-state expectation value of any observable is a unique fuctional of the ground-state density.

The HK theorem [29] also states that the exact ground-state energy can be obtained by minimization of the energy functional defined as

$$E[n] := \big\langle \Psi[n] | (\hat{T} + \hat{V}_{\rm ee} + \hat{V}_{\rm ext}) | \Psi[n] \big\rangle = F_{\rm HK}[n] + \int d\mathbf{r}\, n(\mathbf{r}) V_{\rm ext}(\mathbf{r}), \tag{3.2}$$

where $F_{\mathrm{HK}}[n] = \big\langle \Psi[n] | (\hat{T} + \hat{V}_{\mathrm{ee}}) | \Psi[n] \big\rangle$ is a universal functional of $n(\mathbf{r})$ in the sense that it requires no explicit knowledge of $V_{\mathrm{ext}}(\mathbf{r})$. However, $F_{\mathrm{HK}}[n]$ is defined only for v-representable (VR) densities being in correspondence with external potentials through the HK map (see Sec. 3.4). Levy [30] and Lieb [31] showed that the domain can be extended beyond the VR densities using constrained minimization with a new functional

$$F[n] := \min_{\Psi \to n} \big\langle \Psi[n] | (\hat{T} + \hat{V}_{\mathrm{ee}}) | \Psi[n] \big\rangle, \tag{3.3}$$

which is defined for all N-representable densities. On the grounds of the variational principle, the minimum value of the energy functional (3.2) still equals the correct ground-state energy. The constrained search does not, however, provide the mapping $n(\mathbf{r}) \to V_{\mathrm{ext}}(\mathbf{r})$.

Since the exact form of $F[n]$ is not known, the ground-state density can be found by using a separation originally introduced by Kohn and Sham [32],

$$F[n] = T_0[n] + \frac{1}{2} \int d\mathbf{r}\, n(\mathbf{r}) V_{\mathrm{H}}(\mathbf{r}) + E_{\mathrm{xc}}[n], \tag{3.4}$$

where $T_0[n]$ is the kinetic energy of *noninteracting* electrons, $V_{\mathrm{H}}(\mathbf{r})$ is the classical electrostatic (Hartree) potential of the electrons, and $E_{\mathrm{xc}}[n]$ defines the exchange-correlation energy that contains the many-body effects. The variation of the energy functional yields

$$\frac{\delta E[n]}{\delta n(\mathbf{r})} = \frac{\delta T_0}{\delta n(\mathbf{r})} + V_{\mathrm{ext}}(\mathbf{r}) + V_{\mathrm{H}}(\mathbf{r}) + \frac{\delta E_{\mathrm{xc}}[n]}{\delta n(\mathbf{r})} = \mu, \tag{3.5}$$

where μ is the Lagrange multiplier for the condition of constant electron number. An effective potential is defined as

$$V_{\mathrm{eff}}(\mathbf{r}) := V_{\mathrm{ext}}(\mathbf{r}) + V_{\mathrm{H}}(\mathbf{r}) + V_{\mathrm{xc}}(\mathbf{r}), \tag{3.6}$$

where the Hartree and the exchange-correlation potentials are given by

$$V_{\mathrm{H}}(\mathbf{r}) = \int d\mathbf{r}' \frac{e\, n(\mathbf{r}')}{4\pi\epsilon_0 |\mathbf{r} - \mathbf{r}'|} \quad \text{and} \quad V_{\mathrm{xc}}(\mathbf{r}) = \frac{\delta E_{\mathrm{xc}}[n]}{\delta n(\mathbf{r})}. \tag{3.7}$$

Now the Euler equation (3.5) reads

$$\frac{\delta E[n]}{\delta n(\mathbf{r})} = \frac{\delta T_0}{\delta n(\mathbf{r})} + V_{\mathrm{eff}}(\mathbf{r}) = \mu, \tag{3.8}$$

which is mathematically similar to the true noninteracting case where $V_{\mathrm{eff}}(\mathbf{r})$ is replaced by $V_{\mathrm{ext}}(\mathbf{r})$. The many-electron problem is now described by individual electrons moving in the effective potential.

A further minimization with respect to the orthonormal Kohn-Sham (KS) orbitals ψ_i gives the effective single-electron Schrödinger equation

$$\left[-\frac{\hbar^2}{2m}\nabla^2 + V_{\rm eff}(\mathbf{r})\right]\psi_i(\mathbf{r}) = \epsilon_i\psi_i(\mathbf{r}), \tag{3.9}$$

which finally yields the electron density

$$n(\mathbf{r}) = \sum_{i=1}^{N} |\psi_i(\mathbf{r})|^2. \tag{3.10}$$

Above, the sum runs over the N lowest eigenvalues in accordance with the Pauli exclusion principle. The self-consistent KS equations (3.6,3.9,3.10) can be solved iteratively, and the total energy is calculated from

$$E_{\rm tot} = T_0[n] + \int d\mathbf{r}\, n(\mathbf{r})\left[\frac{1}{2}V_{\rm H}(\mathbf{r}) + V_{\rm ext}(\mathbf{r}) + V_{\rm xc}(\mathbf{r})\right], \tag{3.11}$$

where

$$T_0[n] = -\frac{\hbar^2}{2m}\sum_{i=1}^{N}\langle\psi_i|\nabla^2|\psi_i\rangle = \sum_{i=1}^{N}\epsilon_i - \int d\mathbf{r}\, n(\mathbf{r})V_{\rm eff}(\mathbf{r}). \tag{3.12}$$

Apart from the problems concerning the v-representability [33], the KS scheme of the standard DFT presented above is in principle an exact method for determining the *total energies* and *densities* of an interacting electron system. The KS states (ψ_i, ϵ_i) do not have a direct physical meaning, but they can be useful in describing band structures in solids and also in sketching complicated dynamics in highly correlated quantum dots (see Sec. 4(b) in Publication 6). The most serious practical problem in the DFT calculations arises from the exchange-correlation energy $E_{\rm xc}$ that needs to be approximated in the calculations.

3.2 Generalizations of the theory

The DFT was extended to systems in external magnetic fields by von Barth and Hedin [34], who introduced the spin-density-functional theory (SDFT). It includes the effects of spin polarization in the formalism presented above. The single-electron Schrödinger equation for the spin-up ($\sigma =\uparrow$) and spin-down ($\sigma =\downarrow$) KS states becomes

$$\left[\frac{1}{2m}(\mathbf{p} + e\mathbf{A}(\mathbf{r}))^2 + V_{{\rm eff},\sigma}(\mathbf{r})\right]\psi_{i,\sigma}(\mathbf{r}) = \epsilon_{i,\sigma}\psi_{i,\sigma}(\mathbf{r}), \tag{3.13}$$

where

$$V_{\mathrm{eff},\sigma}(\mathbf{r}) = V_{\mathrm{ext}}(\mathbf{r}) + V_{\mathrm{H}}(\mathbf{r}) + V_{\mathrm{xc},\sigma}(\mathbf{r}), \tag{3.14}$$

and the spin densities are calculated from

$$n_\sigma(\mathbf{r}) = \sum_{i=1}^{N_\sigma} |\psi_{i,\sigma}(\mathbf{r})|^2. \tag{3.15}$$

A fundamental problem of the SDFT is the fact that the external and the exchange-correlation potentials are not uniquely determined by the spin densities. This was pointed out already von Barth and Hedin [34], but the problem was not generalized to the many-body case until recently by Capelle and Vignale [35]. They obtained examples of both systematic and accidental nonuniqueness in the SDFT, implying the nondifferentiability of the universal energy functional $F[n_\uparrow, n_\downarrow]$. By now, any consequences of the nonuniqueness to the accuracy of the SDFT have not been reported. Moreover, it seems that the problem is insignificant for the ground-state properties of systems with well-defined potentials.

In the SDFT the interaction of the magnetic field with the electron current is neglected, although it may become significant at high magnetic fields. To include this coupling, Vignale and Rasolt [36] constructed the so-called current-spin-density-functional theory (CSDFT). The physical (gauge-invariant) orbital current density can be written as a sum of the paramagnetic and diamagnetic current densities,

$$\mathbf{j}(\mathbf{r}) = \mathbf{j}_p(\mathbf{r}) + \frac{e}{m} n(\mathbf{r})\mathbf{A}(\mathbf{r}), \tag{3.16}$$

where the paramagnetic component is given by

$$\mathbf{j}_p(\mathbf{r}) = -\frac{i\hbar}{2m} \sum_{i,\sigma} \left(\psi^*_{i,\sigma} \nabla \psi_{i,\sigma} - \psi_{i,\sigma} \nabla \psi^*_{i,\sigma} \right). \tag{3.17}$$

According to the CSDFT version of the HK theorem, the external scalar and vector potentials V_{ext} and $\mathbf{A}(\mathbf{r})$ are determined, within a trivial additive constant, by the ground-state electron and paramagnetic current densities $n(\mathbf{r})$ and $\mathbf{j}_p(\mathbf{r})$. This generalization of the original DFT suffers, however, from similar nonuniqueness problems as the SDFT [37].

3.3 Local spin-density approximations

As mentioned above, most practical problems of the density-functional methods arise from the unknown exchange-correlation potential. A usual approximation for $V_{\mathrm{xc}}(\mathbf{r})$, especially in 2D systems, is the local density approximation that can

be formulated as follows. At a specific point with a well-defined electron density, an electron is assumed to experience the same many-body response of the surrounding electrons as if they had the same density throughout the entire space as that at the given electron. If the electron spin is taken in to account, the corresponding local spin-density approximation (LSDA) can be expressed as

$$V_{\mathrm{xc}}^{\sigma}(\mathbf{r}) \simeq \frac{\delta E_{\mathrm{xc}}^{\mathrm{LSDA}}}{\delta n_{\sigma}(\mathbf{r})} = \int \mathrm{d}\mathbf{r}\, n(\mathbf{r}) e_{\mathrm{xc}}(n(\mathbf{r}), \zeta(\mathbf{r})), \tag{3.18}$$

where e_{xc} is the exchange-correlation energy per electron in a uniform 2DEG of the density $n = n_{\uparrow} + n_{\downarrow}$ and spin polarization $\zeta = (n_{\uparrow} - n_{\downarrow})/n$. There exists several parametrizations for e_{xc} based on QMC simulations. In Publication III, different expressions for that quantity are compared, namely, the commonly used form of Tanatar and Ceperley [38] and the recent parametrization by Attaccalite and co-workers [39]. The latter was formulated on the basis of fixed-node diffusion Monte Carlo calculations over the whole range of spin polarization ($0 \leq \zeta \leq 1$). The parametrization fulfills the exact results at the low and high-density limits in the 2DEG [40], and it is given as

$$e_{\mathrm{xc}}(r_s, \zeta) = e_x(r_s, \zeta) + (e^{-\beta r_s} - 1) e_{\mathrm{x}}^{(6)}(r_s, \zeta) + \alpha_0(r_s) + \alpha_1(r_s)\zeta^2 + \alpha_2(r_s)\zeta^4. \tag{3.19}$$

In the above expression, the exchange energy is written as

$$e_{\mathrm{x}}(r_s, \zeta) = -2\sqrt{2}[(1+\zeta)^{3/2} + (1-\zeta)^{3/2}]/3\pi r_s. \tag{3.20}$$

In these equations, $r_s = 1/\sqrt{\pi n}$ is the density parameter for the 2DEG with an electron number density n, α's are density-dependent functions of the generalized Perdew-Wang form [41], $\beta = 1.3386$, and $e_{\mathrm{x}}^{(6)}$ is the Taylor expansion of e_x beyond the fourth order in ζ at $\zeta = 0$.

In zero magnetic field, the above parametrization is considerably more accurate than the form of Tanatar and Ceperley [38]. In Publication III, the SDFT results are compared to the VMC calculations of a parabolic six-electron quantum dot in the weak-confinement limit. The situation corresponds to a relatively high exchange-correlation energy in the KS problem. The origin of the better agreement with the VMC results is in the lowered total energy of the fully polarized state. The improvement is also directly proportional to the amplitude of the electron density, which agrees with the result of Gori-Giorgi *et al.* [40]

In the CSDFT formalism, the exchange-correlation energy depends also on the paramagnetic current density $\mathbf{j}_p(\mathbf{r})$. The dependence can be replaced with that on the vorticity defined as [36]

$$\gamma = \nabla \times \frac{\mathbf{j}_{\mathrm{p}}(\mathbf{r})}{n(\mathbf{r})}\bigg|_z. \tag{3.21}$$

The exchange-correlation scalar and vector potentials are written as

$$V_{\mathrm{xc},\sigma} = \frac{\partial(ne_{\mathrm{xc}})}{\partial n_\sigma} \quad \text{and} \quad \mathbf{A}_{\mathrm{xc}} = \frac{1}{n}\left(\frac{\partial}{\partial y}\frac{\partial(ne_{\mathrm{xc}})}{\partial \gamma}, -\frac{\partial}{\partial x}\frac{\partial(ne_{\mathrm{xc}})}{\partial \gamma}, 0\right). \tag{3.22}$$

The accuracy of the calculations depends now on the approximations used for e_{xc} at different magnetic fields. At low fields the currents are negligible, so that $\mathbf{A}_{\mathrm{xc}}$ is close to zero and the formalism reduces to the SDFT, for which the parametrization of Eq. (3.19) can be used. For the strong-field limit there are several reliable results corresponding to the fully polarized 2DEG [42]. The problem is to find accurate interpolation forms between these limits for a given spin polarization, so further simulation data in this regime is needed. However, a good agreement with the VMC results is obtained using the Padé interpolation of Ferconi and Vignale [43] with the above zero-field parametrization of Attaccalite and coworkers [39].

In the case of a parabolic confining potential, the CSDFT is generally found to be an improvement over the SDFT already at relatively low magnetic fields. The differences between the SDFT and VMC energies are, however, rather small. This can be seen in Fig. 3(b) of Publication III, where the relative difference between the SDFT and VMC energies for a six-electron quantum dot with $\hbar\omega_0 = 5$ meV remains below 0.6 % for magnetic fields $B = 0 \ldots 11$ T. For comparison, the UHF results presented in Ref. [44] for a similar system deviate over 4 % from the diffusion Monte Carlo (DMC) (and VMC) energies. Furthermore, we have found that the SDFT predicts the qualitative high-field behavior similarly to the CSDFT in the systems considered in this thesis work. Namely, the accuracy of the SDFT is pronounced in systems with a hard-wall confinement, where the relative contribution of the exchange-correlation to the total energy is smaller than in parabolic systems. Hence, as a computationally more convenient method the SDFT has been used in computing most of the results presented in this thesis for non-zero magnetic fields.

3.4 Ensemble–v-representable densities

As discussed in Sec. 3.1, the cornerstone of the DFT is the mapping between the electron density and the external potential, i.e., $n(\mathbf{r}) \Longleftrightarrow V_{\mathrm{ext}}(\mathbf{r})$. However, $V_{\mathrm{ext}}(\mathbf{r})$ determines $n(\mathbf{r})$ uniquely if and only if the ground state is nondegenerate. Levy [30] found examples of densities that could not be reproduced as nondegenerate and noninteracting ground-state densities of any $V_{\mathrm{ext}}(\mathbf{r})$, but as weighted averages of densities of degenerate ground states corresponding to a $V_{\mathrm{ext}}(\mathbf{r})$. These densities are called ensemble–v-representable densities (E-VR) in contrast to the more common pure-state–v-representable densities (P-VR) that

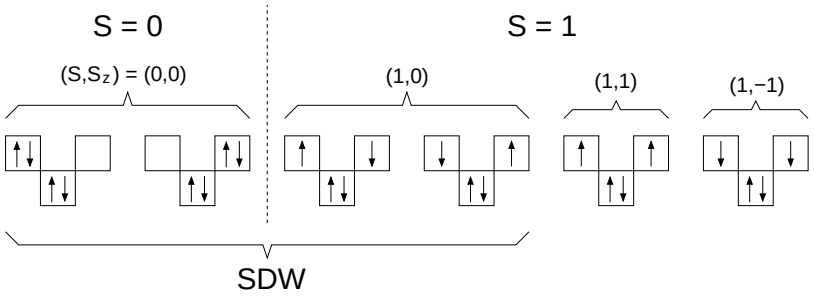

Figure 3.1: Different electron occupations for the $S = 0$ and $S = 1$ states in a four-electron rectangular quantum dot. The SDW state is an incorrect linear combination of the true $S = 0$ state and the $S_z = 0$ configurations of the $S = 1$ state.

can be represented by the density of a single-determinant ground state of noninteracting electrons in a potential $V_{\text{eff}}(\mathbf{r})$ [45].

The underlying problem is the fact that the DFT cannot properly describe E-VR densities, i.e., systems with more than one major configuration in the ground-state wave function. If the spin is unrestricted like in the SDFT, a possible result is a spin-density wave (SDW) [46] with a broken spin symmetry. The result may consist of a nonphysical mixture of different spin states as was first remarked by Hirose and Wingreen [47]. An example of such a system is the four-electron rectangular quantum dot studied in Publication IV using both the SDFT and the ED. It is shown explicitly that the total density of the SDW solution, appearing in the SDFT solution of the $S = 0$ state when the side-length ratio β of the dot is close to one, includes the $S_z = 0$ configurations from the $S = 1$ state. Here S denotes the total spin and S_z is the z component of the total spin. The mixing is illustrated in Fig. 3.1, showing the electron occupations of the $S = 0$ and $S = 1$ states in the dot. The true $S = 0$ state consists of two configurations having equal weights at $\beta = 1$, and the $S = 1$ state has three different S_z states degenerate in energy. The SDW density resembles the ED result for an artificial sum of all the four $S_z = 0$ configurations. Moreover, the comparison of the total energies shows that the SDW solution overcorrects the constant error apparent between the SDFT and ED solutions. On the other hand, the symmetry-restricted ($n_\uparrow = n_\downarrow$) DFT solution deviates even more from the ED energy than the SDW solution. At $\beta \sim 1.2$ the degeneracy of the highest occupied orbitals is sufficiently lifted, and the DFT system transfers from E-VR to P-VR and reproduces the behavior of the ED energy as a function on β.

In rotationally symmetric potentials the concept of broken spin symmetries raises a fundamental problem actively discussed in the literature [48]: The many-body

wave function of a confined system should retain the symmetry of the Hamiltonian. Since in an ideal quantum dot the external potential is kept fixed, the broken-symmetry solutions of circular quantum dots differ crucially from those found in fermion clusters [49] or nuclear [50] systems, in which the lowest-energy configuration can be obtained in accordance with the Jahn-Teller theorem. Therefore, particular care needs to be stressed on the interpretation of the SDW states which in many quantum-dot systems represent energetically reasonable solutions. The same applies to charge-density waves (CDW) that can be considered as particular states of infinite number of degenerate solutions corresponding to arbitrary rotations [28]. The true many-electron wave function is, however, circularly symmetric, unless there are impurities or non-circular boundaries present in the system.

In the above example of a rectangular quantum dot, a possible scheme to avoid the wrong mixing and extend the DFT to the E-VR system is the following. First, a symmetry-restricted calculation is performed with fractional occupation numbers, giving the density $n(\mathbf{r})$ that consists of the core KS orbital ψ_0 and the two higher-energy orbitals ψ_1 and ψ_2 with fractional occupation numbers. Then, two new configurations with the same density $n(\mathbf{r})$ and $S = S_z = 0$ are constructed. Finally, the coupling of this two-fold ensemble is approximated by

$$\delta = \int \phi_+^*(\mathbf{r}_1)\phi_+^*(\mathbf{r}_2)\frac{1}{r_{12}}\phi_-(\mathbf{r}_1)\phi_-(\mathbf{r}_2)\, d\mathbf{r}_1 d\mathbf{r}_2, \tag{3.23}$$

where $\phi_\pm$ are the adequate norm-preserving combinations of ψ_1 and ψ_2, indicating the highest orbitals in the new ensemble. δ gives now directly the energy difference between the symmetry-restricted DFT solution and the *correct* SDFT energy of the $S = 0$ state.

Chapter 4

Real-space multigrid method

The numerical method employed in this thesis to solve the self-consistent KS equations (3.13–3.15) is based on a real-space representation of wave functions, potentials, and densities. It can be considered as an alternative to the conventional plane-wave method, in which the electronic wave functions are written as products of a periodic and a wave-like part, and the periodic part is then expanded using a finite number of plane waves in the momentum space [51]. The benefits of the real-space method are the ability to treat varying length scales and the independence of the periodic boundary conditions. In fact, there are no implicit symmetry restrictions, so the external potential can be shaped arbitrarily in the computing region. This makes the method suitable for conditioning finite asymmetric systems.

In the real-space representation the functions are given their values on a two-dimensional point grid, and the derivatives in the KS equations are converted to finite-difference operators. In practical calculations, the number of grid points is set between 80 and 128 in one direction. This gives ~ 1 nm for a typical grid spacing, which is sufficient for describing electrons in GaAs, and the discretizations are of the 4th order. The accuracy of the calculations reported in this thesis has been checked with the Richardson extrapolation, leading to a typical error of less than $\sim 1\%$ in the total energy ($\lesssim 3\%$ in the low-density limit).

The numerical process in solving the KS equations in real-space grids can be efficiently accelerated with multigrid methods [52]. The main idea is to avoid the critical slowing-down phenomenon that occurs in the relaxation process as the high-frequency error of the grid is reduced rapidly in contrast to the low-frequency components, which converge slowly and thus dominate the error reduction rate. The critical slowing-down is due to the rather short range of the discretization operators to collect information on the grid at a time. In the multigrid methods

the coarser grids are used to eliminate the slowly-oscillating part of the error. The correction can then be interpolated to finer grid. Further iterations are applied to remove the error components on the fine grid induced by the coarse-grid correction.

A reasonable strategy to employ multigrid methods in the KS problem is to begin by solving the wave functions non-self-consistently starting from the coarsest grid and moving gradually to finer grids. Thereafter, the density and the effective potential are updated, and the iteration is continued by performing a V-cycle (fine $\rightarrow$ coarse $\rightarrow$ fine grid) of the wave functions. Then the updates of the potential and the wave functions alternate until the self-consistent solution is obtained. This takes typically $100 \ldots 500$, in difficult cases even thousands of iterations. An adequate alternative to the simple trilinear mixing of the potentials would most likely reduce the number of iterations needed. The most promising technique to improve the convergence is based on the density-response functions [53], probably to be applied for the present method in the near future.

The difficulties in solving the single-electron Schrödinger equation (3.13) are the large amount of eigenpairs that need to be solved and the nonlinearity of the problem, i.e., the error does not obey the same differential equation. A suitable approach is the Rayleigh quotient multigrid (RQMG) method, introduced by Mandel and McCormick [54] for the solution of the eigenpair corresponding to the lowest eigenvalue. The method has been successfully generalized to a desired number of lowest eigenenergy states by Heiskanen *et al.* [55] using penalty functionals on the coarse levels and orthogonalization on the finest level. The method forms the numerical basis of the calculations performed for this thesis.

Chapter 5

Non-circular quantum dots

5.1 Wigner crystallization

In 1934 Wigner [56] predicted that electrons moving in a uniform background of positive charge would localize and form a regular lattice at sufficiently low densities. The reason is the different scaling of the potential and kinetic energies as a function of the electron density. When the electron density decreases, the potential energy becomes gradually dominant and the system crystallizes such that the kinetic energy remains in the zero-point motion of the vibrational modes. The phenomenon was observed experimentally for the first time in the 1970s on the surface of helium droplets cooled to very low temperature [57]. In recent years, quasi-two-dimensional electron systems on liquid helium have attracted particular interest, since they have been suggested as manageable sets of qubits in a quantum computer [58].

The crossover from the Fermi liquid to the Wigner crystal in the 2DEG was studied with Monte Carlo simulations by Tanatar and Ceperley [38], who found a crystallized state at densities with $r_s \gtrsim 37$ (see Sec. 3.3) in the units of the effective Bohr radius $a_B^* = \hbar^2\epsilon/m^*e^2$. In realistic systems, however, the measured crystallization density is considerably larger [59], corresponding to smaller r_s. Chui and Tanatar [60] explained the experimental data with an impurity model, resulting in $r_s \approx 7.5$ for the critical density parameter between the two phases. This value is of the same order of magnitude as in finite quantum-dot systems, studied theoretically with a variety of techniques by several authors [25,26,61–64].

The onset of the Wigner-molecule formation in quantum dots can be determined following several attributes, e.g., the shell-structure formation, properties of the pair-correlation function, changes in the energy spectra [25], or probability densities of single electrons [26]. Creffield and co-workers [61] studied polygonal two-

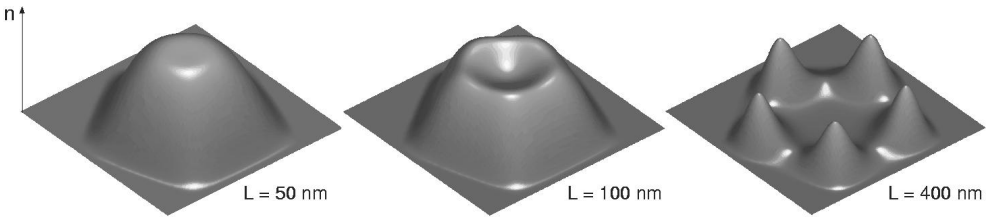

Figure 5.1: Electron densities for three different sizes of a pentagonal two-electron quantum dot. As the size of the dot increases, the electrons localize in the corners and form a Wigner molecule.

electron quantum dots with the ED and connected the Wigner crystallization to the appearance of a local density minimum at the center of the dot.

In Publication I, the Wigner crystallization in polygonal (triangle, square, pentagon, and hexagon) quantum dots containing up to 12 electrons is studied with the SDFT. The external potential is written simply as

$$V_{\text{ext}}(x,y) = \begin{cases} 0, \text{ in the dot} \\ \infty, \text{ elsewhere,} \end{cases} \tag{5.1}$$

and the density parameter is now defined as $r_s = \sqrt{A/(N\pi)}$, where A is the area of the polygon. In the two-electron case, the above-mentioned criterion by Creffield *et al.* [61] for the Wigner crystallization is applied. The ED and SDFT results agree well, giving both $r_s \approx 3$ for the critical density parameter. At larger dot sizes, the electrons localize in the corners to minimize the Coulomb interaction, which is the dominating contribution to the total energy at low densities. The electron density of a pentagonal two-electron dot with different side lengths is shown in Fig. 5.1.

When $N > 2$, the criterion by Creffield and co-workers for the Wigner crystallization cannot be applied, since the electron density is always larger in the corners than at the center of the dot. At sufficiently low densities, however, the formation of "extra" density peaks along the sides of the dot can be observed. In the case of a double number of electrons with respect to the number of corners in the dot, the enlargement of the dot area leads to N density peaks at $r_s \simeq 4.0$ in all polygonal quantum dots studied. This value is defined as the critical density parameter for the Wigner crystallization in those systems. The requirement for the formation of the last density peaks is a broken spin symmetry resulting from the SDFT. We have not analyzed the nature of these SDW-like solutions with the scheme presented in Sec. 3.4. However, we suppose that the origin of the low-density process is different from the symmetry breaking in a rectangular quantum dot, where it was induced by the E-VR problem of the SDFT.

5.2 Effects of deformation

Etching techniques in the fabrication of vertical quantum dots (see Sec. 2.1) provide a controlled way to create dots of different geometries. Austing *et al.* [65] performed experiments on three rectangular mesas with different deformation parameters and measured the addition energy spectra. Furthermore, the confinement was simulated with an elliptic potential and some common features in the spectra were found.

Publication II presents a detailed study on the electronic structure of rectangular quantum dots with a hard-wall confinement potential similar to the previous polygonal system, i.e.,

$$V_{\text{ext}}(x,y) = \begin{cases} 0, & 0 \le x \le \beta L,\ 0 \le y \le L \\ \infty, & \text{elsewhere.} \end{cases} \tag{5.2}$$

The deformation parameter β thus determines the ratio between the side lengths of the rectangle, and the area of the rectangle is set to $\beta L^2 = \pi^2 {a_B^*}^2 \approx 1000\,\text{nm}^2$. The single-electron eigenfunctions can be written using the two quantum numbers n_x and n_y. The energy eigenvalues are given as

$$E_{n_x,n_y} = \frac{1}{2}\left(\frac{n_x^2}{\beta} + \beta n_y^2\right). \tag{5.3}$$

As β increases, the degeneracies at $\beta = 1$ are lifted, and in the quasi-one-dimensional (high-β) limit the occupation is determined by the quantization in the longer direction to the states $(n_x, 1)$.

The chemical potentials and the addition energies, defined in Sec. 2.2, are calculated as a function of β with both the SDFT and VMC. The agreement between the results of the two methods is very precise. In addition, the comparison of our results with the experiments and previous simulations [65] shows that the hard-wall approximation is slightly more realistic than the elliptic one. However, more experimental data over a wider range of β would be needed. A comprehensive experiment would contain a way to tune β for a single sample.

The ground-state spin structure of the many-electron system has an interesting behavior as a function of β and the electron number N. Near the degenerate points of the corresponding single-electron spectrum, there is partial spin polarization ($S = 1$) in agreement with Hund's rule. In most cases, the polarization occurs at higher β than a crossing of the corresponding single-electron states, indicating a lower effective deformation in the interacting system than that of the bare external potential. Due to the hard-wall confinement, the role of the electron-electron interactions is thus opposite to the elliptic case considered by Lee *et*

al. [66] According to our calculations, the $S = 1$ states are bracketed by SDW solutions, in which the spin-up and spin-down densities are symmetrically coupled with each other. As presented in Sec. 3.4 for the four-electron case (Publication IV), they result from the E-VR problem of the SDFT, leading to a wrong mixing of different spin states.

In the quasi-one-dimensional limit the rectangular dot forms, depending on the values of β and the density parameter r_s, a charge-density wave (CDW) or a SDW with $N/2$ or N density maxima, respectively. At particularly large values of β and r_s, there is also a transition to a fully polarized state similarly to very thin three-dimensional metal nanowires [67]. The density-wave structures differ considerably from those of the elliptic nanowires studied be Reimann *et al.* [68] In the present hard-wall case, the Coulomb force pushes the dominant electron distribution to the both ends of the wire, contrary to the elliptic wires defined by a bowl-like external confinement. Another consequence from the different potential is the the absence of CDW's in the symmetry-restricted solutions of elliptic wires.

5.3 Magnetic field effects

Until now, theoretical studies of interacting electrons in non-circular quantum wells in the presence of an external magnetic field have been limited to rather small electron numbers. Creffield *et al.* [69] found Aharonov-Bohm-type oscillations in the lowest levels of a square two-electron quantum dot, indicating periodic singlet-triplet changes in the ground state. Ugajin [70] showed that these transitions lead to strong effects in the optical excitation spectra. Square geometries have also been studied in connection with FIR calculations [11–13], and the effects of the interactions on the magnetization have been evaluated [71, 72].

5.3.1 Chaotic properties

Non-circular single-electron systems in magnetic fields have attracted a lot of interest as regards to nonintegrable quantum billiards [73]. Its origin lies in the studies of the classical behavior of confined particles in a uniform magnetic field [74]. Nakamura and Thomas [75] studied the chaotic behavior in elliptic quantum billiards and considered especially its manifestation in the diamagnetic susceptibility. Their work was specified by von Oppen [76], who analyzed the mesoscopic susceptibility of square billiards and found consistent results with the experiment performed for GaAs squares by Lévy *et al.* [77] Even if there are exceptions [78], the statistical properties of quantum levels usually reflect the integrability of the corresponding classical system. Namely, the Poisson or Wigner distributions for

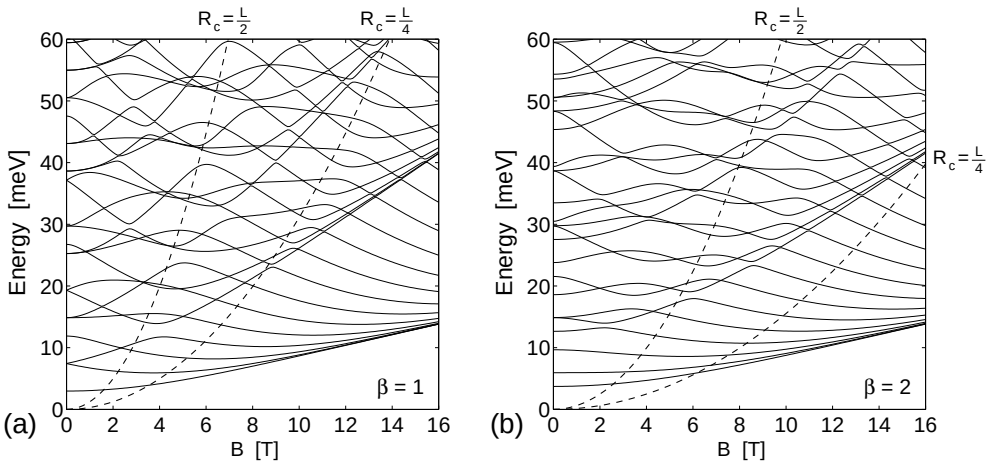

Figure 5.2: Lowest noninteracting single-electron eigenenergies for rectangular quantum dots with $\beta = 1$ (a) and $\beta = 2$ (b).

the energy-level spacings are obtained in the case of an integrable and a classically chaotic system, respectively [73]. The nature of the dynamics depends on the strength of the applied magnetic field as was shown for a stadium-shaped quantum dot by Ji and Berggren [79]. A detailed analysis has been performed also for the rectangular billiards penetrated by a flux line [80]. Classically this represents a so-called pseudointegrable system.

The single-electron Hamiltonian (2.1) for a rectangular quantum dot is written in a component form as

$$H_0 = -\frac{\hbar^2}{2m^*}\left(\frac{\partial^2}{\partial x^2} + \frac{\partial^2}{\partial y^2}\right) - \frac{i\hbar eB}{4m^*}\left(x\frac{\partial}{\partial y} - y\frac{\partial}{\partial x}\right) + \frac{e^2B^2}{4m^*}\left(x^2 + y^2\right) + V_{\text{ext}}(x, y), \tag{5.4}$$

where the external potential is similar to Eq. (5.2), and the dot area is set to $4\pi^2\, {a_B^*}^2 \approx 4000\,\text{nm}^2$. Due to the lack of circular symmetry, the angular momentum is not conserved and the corresponding eigenvalue problem is not analytically solvable at finite, non-zero B. However, we have solved the discretized eigenvalue equation (2.2) for the 25 lowest states numerically on a 2D point grid using the RQMG method introduced in Sec. 4.

Figure 5.2 shows the spectra for rectangular quantum dots with $\beta = 1$ (square) and $\beta = 2$ in magnetic fields up to 16 T. There are several avoided crossings between those states that correspond to a similar symmetry. The level repulsion obviously pushes the distribution of the energy-level spacings toward the Wigner

picture [73]. A statistical analysis of the energy levels is not, however, included in this examination. At high B the system becomes integrable and the eigenstates condense into Landau levels similarly to the circular systems considered in Sec. 2.3.

The classical dynamics of confined, noninteracting electrons in a magnetic field can be analyzed by comparing the effective cyclotron radius $R_c = m^*v/B$ to the dimensions of the dot [74]. The criterion of having at least one integrable component of motion in the system is $R_c \leq \rho_{max}$, where ρ_{max} is the radius of the largest possible circular orbit enclosed by the boundary. Using $E = \frac{1}{2}m^*v^2$ for a classical electron and $\rho_{max} = L/2$, yields $E \gtrsim L^2B^2/8m^*$ for the classically chaotic regime in the system. These limits as well as the cases $R_c = L/4$ are shown as dashed lines in Fig. 5.2. It is obvious from the figure that the scaling of the quantum-chaos borderline as a function of β is very different from the chaos borderline in the classical picture. Namely, both cases ($\beta = 1, 2$) represent nearly similar Landau-level condensation and the disappearance of avoided crossings as B increases. Hence, the dot area is the determining parameter for the quantum chaotic behavior instead of β. The main difference in Figs. 5.2(a) and 5.2(b) is the curvature of the energy levels, becoming smaller as β increases. This corresponds to the reduction in the diamagnetic susceptibility in agreement with the results by Nakamura and Thomas [75] for elliptic geometries.

The development of individual eigenstates as a function of B can be illustrated with the probability densities $n = |\psi|^2$ and the current densities defined as

$$\mathbf{j} = \frac{i\hbar}{2m^*}(\psi\nabla\psi^* - \psi^*\nabla\psi) + \frac{e}{m^*}\mathbf{A}|\psi|^2. \tag{5.5}$$

Figure 5.3 shows the structure of the 15th state at $B = 2$ and 16 T, corresponding to chaotic and regular dynamics, respectively. In the latter case, the states have condensed into bulk Landau states, and the counter-clockwise current flow corresponds to the classical Lorentz force on the electron [see Figs. 5.3(b) and (d)]. On the contrary, the density structure is highly complex at $B = 2$ T, and there are many current vortices localized at the density minima. As seen in Figs. 5.3(a) and (c), the vortices possess currents in both directions. Due to the high localization of the wave functions in the sharp-angular geometry, we were not able to find smooth clockwise currents around the whole quantum well, i.e., the so-called edge states [81]. For example, in stadium-shaped dots studied by Ji and Berggren [79], there are edge states that have also an experimental realization in the periodic oscillations of the high-B magnetoresistance [82]. Otherwise, the formation of current vortices and the Landau-level condensation are qualitatively similar in stadium-shaped and rectangular geometries.

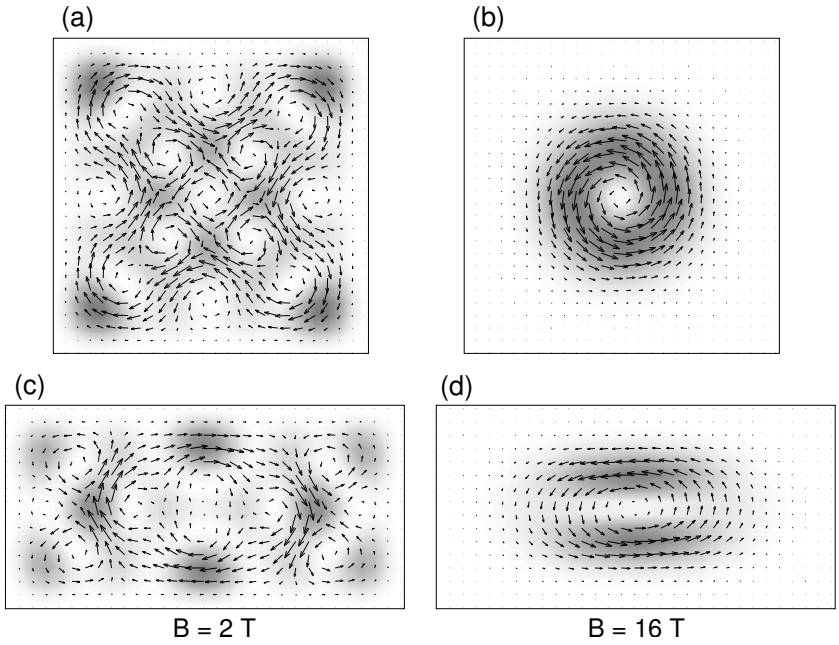

Figure 5.3: Electron and current densities for the 15th lowest state in square and rectangular quantum dots with $B = 2$ T (a, c) and 16 T (b, d). The darker regions correspond to larger electron densities.

5.3.2 Maximum-density-droplet formation

A many-electron quantum dot has identifiable phases in the electronic structure as the strength of the external magnetic field is varied. In a circular geometry, a maximum-density droplet (MDD) is a fully polarized state, in which the electrons occupy successive angular momentum levels from $l = 0$ to $l = -N + 1$, where N is the number of electrons in the dot. Oosterkamp and co-workers [83] observed experimentally that the MDD state is stable for a rather wide range of the magnetic field. At sufficiently high magnetic fields the MDD reconstructs into a lower-density droplet. In the case of a parabolic confinement potential, several possible results for the reconstructed state have been suggested in addition to a symmetry-preserving solution with the electrons occupying the levels $l = -1, -2, ..., -N$ [84]. There are signs of vortex clustering in quantum dots [85], as well as edge fluctuations in forms of strong charge density waves [86,87], Wigner crystalline edges [88], or spin-texturing [89]. Yang *et al.* [90] have used the ED to study the correlations between the interior holes and the edge excitations up to 30 electrons.

In Publications V and VI, the MDD window of hard-wall quantum dots is identified in the calculated chemical potentials of the fully polarized states that become

the lowest in energy at a certain magnetic field strength. The onset of the MDD can also be predicted from the number of flux quanta N_Φ penetrating through the quantum dot. N_Φ depends only on the area of the dot, namely, $N_\Phi = \Phi/\Phi_0$, where the magnetic flux $\Phi = BA$ and $\Phi_0 = h/e$ is the flux quantum. At the MDD formation, the number of flux quanta equals to $N-1$ vortices "seen" by an electron as the other electrons are fixed. A vortex is defined as a point where the wave function is zero and its phase changes by -2π in a counterclockwise rotation [91]. This gives a geometry-independent onset field for the MDD: $B = h(N-1)/eA \approx 1.04(N-1)$. Due to the Coulomb interactions, the MDD electron density in a hard-wall dot is pronouncedly localized in the corners and on the edges, in contrast with the parabolic case showing a smooth density distribution [87].

5.3.3 Oscillations in the high-field limit

As the magnetic field increases, the circular hard-wall MDD reconstructs into a symmetric ring-like structure. The absence of the localized edge states is again due to the shape of the potential that favors a high electron density at the round edge. The total angular momentum thus obtains integer values, growing in steps of N as the magnetic field increases. The ground state remains fully polarized beyond the MDD, i.e., $S_z = N/2$.

The periodic behavior, reflecting the competition between the magnetic confinement and the Coulomb repulsion, is also present in non-circular quantum dots. The electronic structure oscillates between well-localized and more diffuse states as a function of the magnetic field. This variation in the fully polarized ground state is similar to the singlet-triplet oscillations found in interacting two-electron quantum dots of both circular [92] and square [69] shapes, as well as in a double-dot system [93]. The periodicity is also clearly observable in the total magnetization, defined as $M = -\partial E_{\mathrm{tot}}/\partial B$ for a finite system in a zero temperature.

We have analyzed the internal structure of the density oscillations in rectangular quantum dots by considering the expectation values of the angular momentum operator $\hat{l}_z = -i\hbar(x\frac{\partial}{\partial y} - y\frac{\partial}{\partial x})$ for different KS states in the high-B regime. There are clear corner modes in all the systems. However, the orbits in the middle of the dot are found to be very sensitive to the deformation parameter β. A square dot with eight electrons shows a rather regular behavior, whereas in a rectangular dot with $\beta = 2$ there are two different oscillating modes interlocked to each other: (i) periodic localization in the y direction, and (ii) a complex fluctuating structure, reminiscent of a "lozenge" orbit in the corresponding classical bouncing map [94].

5.4 External impurities in quantum dots

Theoretical modeling of quantum dots is usually based on the approximation of clean samples, although in real semiconductor devices the effects due to impurities or donor scattering centers may be remarkable. Even a relatively weak distortion of the circular symmetry has a strong influence on the energy spectrum, e.g., by lifting the degeneracies and inducing level repulsions [95].

In Publication VII, a measured transport spectrum of a vertical quantum dot is shown to have clear deviations from the FD energies. We have reproduced the spectrum using an external model potential $V_{\rm ext} = V_{\rm conf} + V_{\rm imp}$, where the confinement part is of a parabolic form with soft edges, written as

$$V_{\rm conf}(\mathbf{r}) = \begin{cases} \frac{1}{2} m^* \omega_0^2 r^2, & r \le r_c \\ m^* \omega_0^2 \left[s(r - r_c)^2 - r_c(\frac{r_c}{2} - r) \right], & r > r_c, \end{cases} \tag{5.6}$$

where r_c is the cusp radius and s defines the strength of the rounding term. The impurity can be described by a Coulombic potential given as

$$V_{\rm imp}(\mathbf{r}) = \frac{|q|}{4\pi\epsilon_0\kappa\sqrt{(\mathbf{r} - \mathbf{R})^2 + d^2}}, \tag{5.7}$$

where q is the (negative) charge of the impurity particle, κ describes the "dielectricity" between the impurity and the electrons in the quantum dot, and R and d are the lateral and vertical distances of the impurity from the dot center, respectively.

Figure 5.4 shows the measured spectrum and the single-electron energies (dashed lines), numerically calculated from Eq. (2.2) using $V_{\rm ext}$ above with the adjusted parameters. The agreement is generally very good up to the highest levels shown in the spectrum. The parameter values obtained for the best possible fitting indicate a multiple-charged impurity located close to the quantum-dot plane. Due to the grown-induced formation of the quantum dot in the absence of gates around the sample, the confinement is relatively strong, but it becomes considerably softer near the edges ($r \ge r_c$).

We also study the many-electron properties in a similar impurity-containing quantum dot by using the SDFT. As expected from the single-electron spectrum, the impurity evens out the energy evolution as a function of the magnetic field. This is in agreement with the DMC calculations performed for randomly disordered quantum dots by Güçlü *et al.* [44]

The stability of the MDD emerging in the polarized state at sufficiently high magnetic fields is demonstrated by varying the impurity location. As the impurity is brought from infinity to the dot center, the total angular momentum grows

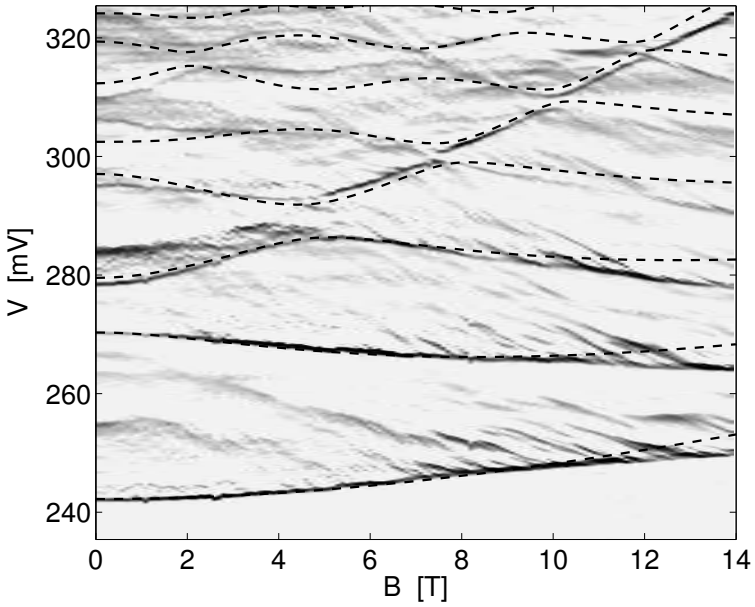

Figure 5.4: Measured transport spectrum of a GaAs/AlGaAs quantum dot and the calculated single-electron energies (dashed lines) corresponding to the model potential given in the text.

smoothly from $|L_z| = N(N-1)/2$ to $N(N-1)/2+N$, corresponding to a change from a perfect MDD to a quantum ring. The variation of R near the center of the dot shows that the many-electron quantum dot tends to preserve the ring-like properties, e.g., periodic oscillations in the total magnetization (see Sec. 5.3.3). This is verified by comparing M in interacting and noninteracting systems. The tendency of the interactions to screen the impurity was also notified by Halonen *et al.* [95], and by Sheng and Xu [72] in their studies for distorted quantum dots containing a small number of electrons ($N \leq 3$).

Chapter 6

Summary

This thesis presents and clarifies the ground-state properties in quantum dots where the external potential confining the electrons is deformed from a circular parabolic geometry. In particular, the effects of the electron-electron interactions and the external magnetic field are considered. The computational method is based on the spin-density-functional theory, which is critically analyzed in connection with the local spin-density approximation and the ensemble–v-representability problem.

Publications I and II deal with the electronic properties of polygonal and rectangular quantum dots in zero magnetic field. In polygonal systems, the Wigner-molecule formation in the low-density limit is determined, and the comparable results for the two-electron system agree well with the exact diagonalization. The addition energy spectra of rectangular hard-wall quantum dots agree astonishingly well with the quantum Monte Carlo calculations. Moreover, the applied geometry is a slightly better approximation for fabricated rectangular quantum dots than the elliptic shape.

In Publication III, different parametrizations of the local spin-density approximation for the electron exchange and correlation are compared. The novel form by Attaccalite and co-workers is found to be a significant improvement over the previous ones in zero magnetic field. Publication IV shows explicitly that the spin-density-functional theory can lead to a wrong mixing of different spin states in systems possessing ensemble–v-representable densities. A simple scheme that corrects the problem is presented.

Publications V and VI consider the effects of the magnetic field on the electronic properties of hard-wall, particularly rectangular quantum dots. In this thesis overview, unpublished results comparing the classically chaotic regimes and the quantum mechanical single-electron eigenstates are also presented. In the

corresponding many-electron problem, the formation of a rather inhomogeneous maximum-density droplet at the expected magnetic field strength is confirmed. The high-field limit is characterized by periodic state oscillations which are highly dependent on the dot geometry.

In Publication VII, an experimental single-electron spectrum containing a clear sign of an external impurity is modeled with a external potential that consists of a smoothed parabolic confinement and a negatively charged impurity placed near the quantum dot. A good agreement between the experiment and the model is found. The many-electron properties, e.g., the development of the spin states and the chemical potentials are studied and compared to clean quantum dots. The behavior in the magnetization shows that the increasing electron number leads to the screening of the impurity.

It is shown that the density-functional theories based on a real-space multigrid method are versatile and efficient tools to examine quantum-dot systems of various geometries and sizes. For the forthcoming studies, several issues presented in this thesis encourage further investigations. First, the nature of the spin-density waves and especially the corrected computational scheme, related to ensemble–v-representable densities, need to be analyzed in a more general manner. Second, the local spin-density approximations, particularly for the current-spin-density-functional theory, ought to be developed further in order to specify the precise role of the electron currents in the presence of a high magnetic field. Third, the study of chaotic properties should be generalized by performing a statistical analysis of the single-electron energies. In addition, the ongoing development with the response-function schemes will presumably lead towards the study of dynamic many-electron properties within the time-dependent density-functional theory. It is naturally hoped that the results presented in this thesis would inspire more theoretical and experimental work on this exciting field of interacting electrons in nanostructures, showing a diversity of often unexpected phenomena.

Bibliography

[1] For an overview, see L. Jacak, P. Hawrylak, and A. Wójs, *Quantum dots* (Springer, Berlin, 1998).

[2] U. Meirav, M. A. Kastner, and S. J. Wind, *Single-Electron Charging and Periodic Conductance Resonances in GaAs Nanostructures*, Phys. Rev. Lett. **65**, 771 (1990).

[3] D. Loss and D. P. DiVincenzo, *Quantum computation with quantum dots*, Phys. Rev. A **57**, 120 (1998).

[4] J. M. Elzerman, R. Hanson, J. S. Greidanus, L. H. Willems van Beveren, S. De Franceschi, L. M. K. Vandersypen, S. Tarucha, and L. P. Kouwenhoven, *A few-electron quantum dot circuit with integrated charge read-out*, Phys. Rev. B **67**, 161308(R) (2003).

[5] M. A. Reed, J. N. Randall, R. J. Aggarwal, R. J. Matyi, T. M. Moore, and A. E. Wetsel, *Observation of Discrete Electronic States in a Zero-dimensional Semiconductor Nanostructure*, Phys. Rev. Lett. **60**, 535 (1988).

[6] S. Tarucha, D. G. Austing, T. Honda, R. J. van der Hage, and L. P. Kouwenhoven, *Shell Filling and Spin Effects in a Few Electron Quantum Dot*, Phys. Rev. Lett. **77**, 3613 (1996).

[7] L. P. Kouwenhoven, D. G. Austing, and S. Tarucha, *Few-electron quantum dots*, Rep. Prog. Phys. **64**, 701 (2001).

[8] S. Fafard, K. Hinzer, S. Raymond, M. M. Dion, J. P. McCaffrey, Y. Feng, and S. Charbonneau, *Red-emitting semiconductor quantum dot lasers*, Science **274**, 1350 (1996).

[9] R. C. Ashoori, *Electrons in artificial atoms*, Nature **379**, 413 (1996).

[10] P. A. Maksym and T. Chakraborty, *Quantum dots in a magnetic field: Role of electron-electron interactions*, Phys. Rev. Lett. **65**, 108 (1990).

[11] R. Ugajin, *Effect of the Coulomb interaction on far-infrared absorption in a square-well quantum dot*, Phys. Rev. B **51**, 10714 (1995).

[12] I. Magnúsdóttir and V. Gudmudsson, *Influence of the shape of quantum dots on their far-infrared absorption*, Phys. Rev. B **60**, 16591 (1999).

[13] M. Valín-Rodríquez, A. Puente, and L. Serra, *Far-infrared absorption in triangular and square quantum dots: Characterization of corner and side modes*, Phys. Rev. B **64**, 205307 (2001).

[14] M. Marlo, A. Harju, and R. M. Nieminen, *Role of Interactions in the Far-Infrared Spectrum of a Lateral Quantum-Dot Molecule*, Phys. Rev. Lett. **91**, 187401 (2003).

[15] A. Kumar, S. E. Laux, and F. Stern, *Electron states in a GaAs quantum dot in a magnetic field*, Phys. Rev. B **42**, 5166 (1990).

[16] N. A. Bruce and P. A. Maksym, *Quantum states of interacting electrons in a real quantum dot*, Phys. Rev. B **61**, 4718 (2000).

[17] M. Stopa, *Quantum dot self-consistent electronic structure and the Coulomb blockade*, Phys. Rev. B **54**, 13767 (1996).

[18] V. Fock, *Bemerkung zur Quantelung des harmonischen Oszillators im Magnetfeld*, Z. Phys. **47**, 466 (1928); C. G. Darwin, *The diamagnetism of the free electron*, Proc. Cambridge Philos. Soc. **27**, 86 (1930).

[19] F. Geerinckx, F. M. Peeters, and J. T. Devreese, *Effect of the confining potential on the magneto-optical spectrum of a quantum dot*, J. Appl. Phys. **68**, 3435 (1990).

[20] A. Fuhrer, S. Lüscher, T. Heinzel, K. Ensslin, W. Wegscheider, and M. Bichler, *Transport properties of quantum dots with steep walls*, Phys. Rev. B **63**, 125309 (2001).

[21] L. Jacak, J. Krasnyj and A. Wójs, *Spin-orbit interaction in the quantum dot*, Physica B **229**, 279 (1997).

[22] S. A. Mikhailov and N. A. Savostianova, *Quantum-dot lithium in the strong-interaction regime: Depolarization of electron spins by a magnetic field*, Phys. Rev. B **66**, 033307 (2002).

[23] M. B. Tavernier, E. Anisimovas, F. M. Peeters, B. Szafran, J. Adamowski, and S. Bednarek, *Four-electron quantum dot in a magnetic field*, Phys. Rev. B **68**, 205305 (2003).

[24] P. A. Maksym and T. Chakraborty, *Effect of electron-electron interactions on the magnetization of quantum dots*, Phys. Rev. B **45**, 1947 (1992).

[25] R. Egger, W. Häusler, C. H. Mak, and H. Grabert, *Crossover from Fermi Liquid to Wigner Molecule Behavior in Quantum Dots*, Phys. Rev. Lett. **82**, 3320 (1999).

[26] A. Harju, S. Siljamäki, and R. M. Nieminen, *Wigner molecules in quantum dots: a quantum Monte Carlo study*, Phys. Rev. B **65**, 075309 (2002).

[27] B. Reusch and H. Grabert, *Unrestricted Hartree-Fock for quantum dots*, Phys. Rev. B **68**, 045309 (2003).

[28] J. R. Trail, M. D. Towler, and R. J. Needs, *Unrestricted Hartree-Fock theory of Wigner crystals*, Phys. Rev. B **68**, 045107 (2003).

[29] P. Hohenberg and W. Kohn, *Inhomogeneous Electron Gas*, Phys. Rev. **136**, B864 (1964).

[30] M. Levy, *Electron densities in search of Hamiltonians*, Phys. Rev. A **26**, 1200 (1982).

[31] E. H. Lieb, *Density functionals for Coulomb systems*, Int. J. Quantum Chem. **24**, 243 (1983).

[32] W. Kohn and L. Sham, *Self-Consistent Equations Including Exchange and Correlation Effects*, Phys. Rev. **140**, A1133 (1965).

[33] For a review, see, e.g., R. M. Dreizler and E. K. U. Gross, *Density Functional Theory* (Springer, Berlin, 1990); R. van Leeuwen, *Density functional approach to the many-body problem: key concepts and exact functionals*, Adv. Quantum Chem. **43**, 24 (2003).

[34] U. von Barth and L. Hedin, *A local exchange-correlation potential for the spin polarized case*, J. Phys. C **5**, 1629 (1972).

[35] K. Capelle and G. Vignale, *Nonuniqueness of the Potentials of Spin-Density-Functional Theory*, Phys. Rev. Lett. **86**, 5546 (2001).

[36] G. Vignale and M. Rasolt, *Density-Functional Theory in Strong Magnetic Fields*, Phys. Rev. Lett. **59**, 2360 (1987).

[37] K. Capelle and G. Vignale, *Nonuniqueness and derivative discontinuities in density-functional theories for current-carrying and superconducting systems*, Phys. Rev. B **65**, 113106 (2002).

[38] B. Tanatar and D. M. Ceperley, *Ground state of the two-dimensional electron gas*, Phys. Rev. B **39**, 5005 (1989).

[39] C. Attaccalite, S. Moroni, P. Gori-Giorgi, and G. B. Bachelet, *Correlation energy and Spin Polarization in the 2D Electron Gas*, Phys. Rev. Lett. **88**, 256601 (2002).

[40] P. Gori-Giorgi, C. Attaccalite, S. Moroni, and G. B. Bachelet, *Two-dimensional electron gas: correlation energy versus density and spin polarization*, Int. J. Quantum Chem. **91**, 126 (2003).

[41] J. P. Perdew and Y. Wang, *Accurate and simple analytic representation of the electron-gas correlation energy*, Phys. Rev. B **45**, 13244 (1992).

[42] R. Price and S. Das Sarma, *Exchange-correlation energy for a two-dimensional electron gas in a magnetic field*, Phys. Rev. B **54**, 8033 (1996), and references therein.

[43] M. Ferconi and G. Vignale, *Current-density-functional theory of quantum dots in a magnetic field*, Phys. Rev. B **50**, 14722 (1994).

[44] A. D. Güçlü, J. S. Wang, and H. Guo, *Disordered quantum dots: A diffusion quantum Monte Carlo study*, Phys. Rev. B **68**, 035304 (2003).

[45] C. A. Ullrich and W. Kohn, *Kohn-Sham Theory for Ground-State Ensembles*, Phys. Rev. Lett. **87**, 093001 (2001).

[46] M. Koskinen, M. Manninen, and S. M. Reimann, *Hund's Rules and Spin Density Waves in Quantum Dots*, Phys. Rev. Lett. **79**, 1389 (1997).

[47] K. Hirose and N. S. Wingreen, *Spin-density-functional theory of circular and elliptical quantum dots*, Phys. Rev. B **59**, 4604 (1999).

[48] S. M. Reimann and M. Manninen, *Electronic structure of quantum dots*, Rev. Mod. Phys. **74**, 1283 (2002).

[49] Häkkinen, J. Kolehmainen, M. Koskinen, P. O. Lipas, and M. Manninen, *Universal Shapes of Small Fermion Clusters*, Phys. Rev. Lett. **78**, 1034 (1997).

[50] S. Frauendorf, *Spontaneous symmetry breaking in rotating nuclei*, Rev. Mod. Phys. **73**, 463 (2001).

[51] M. C. Payne, M. T. Peter, D. C. Allan, T. A. Arias, and J. D. Joannopoulos, *Iterative minimization techniques for ab initio total-energy calculations: molecular dynamics and conjugate gradients*, Rev. Mod. Phys. **64**, 1045 (1992).

[52] T. L. Beck, *Real-space mesh techniques in density-functional theory*, Rev. Mod. Phys. **72**, 1041 (2000).

[53] J. Auer and E. Krotscheck, *A rapidly converging algorithm for solving the Kohn-Sham and related equations in electronic structure theory*, Computer Physics Communications **118**, 139 (1999).

[54] J. Mandel and S. McCormick, *A Multilevel Variational Method for Au = Bu on Composite Grids*, J. Comp. Phys. **80**, 442 (1989).

[55] M. Heiskanen, T. Torsti, M. J. Puska, and R. M. Nieminen, *Multigrid method for electronic structure calculations*, Phys. Rev. B **63**, 245106 (2001).

[56] E. P. Wigner, *On the Interaction of Electrons in Metals*, Phys. Rev. **46**, 1002 (1934).

[57] C. C. Grimes and G. Adams, *Evidence for a Liquid-to-Crystal Phase Transition in a Classical, Two-Dimensional Sheet of Electrons*, Phys. Rev. Lett. **42**, 795 (1979).

[58] P. M. Platzman and M. I. Dykman, *Quantum Computing with Electrons Floating on Liquid Helium*, Science **284**, 1967 (1999).

[59] V. M. Pudalov, M. D'Iorio, S. V. Kravchenko, and J. W. Campbell, *Zero-magnetic-field collective insulator phase in a dilute 2D electron system*, Phys. Rev. Lett. **70**, 1866 (1993).

[60] S. T. Chui and B. Tanatar, *Impurity Effect on the Two-Dimensional-Electron Fluid-Solid Transition in Zero Field*, Phys. Rev. Lett. **74**, 458 (1995).

[61] C. E. Creffield, W. Häusler, J. H. Jefferson, and S. Sarkar, *Interacting electrons in polygonal quantum dots*, Phys. Rev. B **59**, 10719 (1999).

[62] S. M. Reimann, M. Koskinen, and M. Manninen, *Formation of Wigner molecules in small quantum dots*, Phys. Rev. B **62**, 8108 (1999).

[63] C. Yannouleas and U. Landman, *Spontaneous Symmetry Breaking in Single and Molecular Quantum Dots*, Phys. Rev. Lett. **82**, 5325 (1999).

[64] B. Reusch, W. Häusler, and H. Grabert, *Wigner molecules in quantum dots*, Phys. Rev. B **63**, 113313 (2001).

[65] D. G. Austing, S. Sasaki, S. Tarucha, S. M. Reimann, M. Koskinen, and M. Manninen, *Ellipsoidal deformation of vertical quantum dots*, Phys. Rev. B **60**, 11514 (1999).

[66] I. H. Lee, Y. H. Kim, and K. H. Ahn, *Electronic structure of ellipsoidally deformed quantum dots*, J. Phys.: Condens. Matter **13**, 1987 (2001).

[67] N. Zabala, M. J. Puska, and R. M. Nieminen, *Spontaneous Magnetization of Simple Metal Nanowires*, Phys. Rev. Lett. **80**, 3336 (1998).

[68] S. M. Reimann, M. Koskinen, and M. Manninen, *End states due to a spin-Peierls transition in quantum wires*, Phys. Rev. B **59**, 1613 (1999).

[69] C. E. Creffield, J. H. Jefferson, S. Sarkar, and D. L. J. Tipton, *Magnetic field dependence of the low-energy spectrum of a two-electron quantum dot*, Phys. Rev. B **62**, 7249 (2000).

[70] R. Ugajin, *Magneto-optics in a square-well quantum dot*, Phys. Rev. B **53**, 6963 (1996).

[71] I. Magnúsdóttir and V. Gudmudsson, *Magnetization of noncircular quantum dots*, Phys. Rev. B **61**, 10229 (2000).

[72] W. Sheng and H. Xu, *Quantum dots with interacting electrons: Energy spectra and magnetization*, Physica B **256-258**, 152 (1998).

[73] H.-J. Stockmann, *Quantum Chaos: An Introduction*, (Cambridge University Press, Cambridge, 2000).

[74] M. Robnik and M. V. Berry, *Classical billiards in magnetic fields*, J. Phys. A **18**, 1361 (1985).

[75] K. Nakamura and H. Thomas, *Quantum Billiard in a Magnetic Field: Chaos and Diamagnetism*, Phys. Rev. Lett. **61**, 247 (1988).

[76] F. von Oppen, *Magnetic susceptibility of ballistic microstructures*, Phys. Rev. B **50**, 17151 (1994).

[77] L. P. Lévy, D. H. Reich, L. Pfeiffer, and K. West, *Aharonov-Bohm ballistic billiards*, Physica B **189**, 204 (1993).

[78] P. Seba, *Wave chaos in singular quantum billiard*, Phys. Rev. Lett. **64**, 1855 (1990).

[79] Z.-L. Ji and K.-F. Berggren, *Transition from chaotic to regular behavior of electrons in a stadium-shaped quantum dot in a perpendicular magnetic field*, Phys. Rev. B **52**, 1745 (1995).

[80] G. Date, S. R. Jain, and M. V. N. Murthy, *Rectangular billiard in the presence of a flux line*, Phys. Rev. E **51**, 198 (1995).

[81] C. S. Lent, *Edge states in a circular quantum dot*, Phys. Rev. B **43**, 4179 (1991).

[82] C. M. Marcus, A. J. Rimberg, R. M. Westervelt, P. F. Hopkins, and A. C. Gossard, *Conductance fluctuations and chaotic scattering in ballistic microstructures*, Phys. Rev. Lett. **69**, 506 (1992).

[83] T. H. Oosterkamp, J. W. Janssen, L. P. Kouwenhoven, D. G. Austing, T. Honda, and S. Tarucha, *Maximum-Density Droplet and Charge Redistributions in Quantum Dots at High Magnetic Fields*, Phys. Rev. Lett. **82**, 2931 (1999).

[84] S.-R. Eric Yang, A. H. MacDonald, and M. D. Johnson, *Addition spectra of quantum dots in strong magnetic fields*, Phys. Rev. Lett. **71**, 3194 (1993).

[85] H. Saarikoski, A. Harju, M. J. Puska, and R. M. Nieminen, *Vortex Clusters in Quantum Dots*, submitted to Phys. Rev. Lett., cond-mat/0402514.

[86] C. de Chamon and X. G. Wen, *Sharp and smooth boundaries of quantum Hall liquids*, Phys. Rev. B **49**, 8227 (1994).

[87] S. M. Reimann, M. Koskinen, M. Manninen, and B. R. Mottelson, *Quantum Dots in Magnetic Fields: Phase Diagram and Broken Symmetry at the Maximum-Density-Droplet Edge*, Phys. Rev. Lett. **83**, 3270 (1999).

[88] E. Goldmann and S. R. Renn, *Wigner crystalline edges in $\nu \lesssim 1$ quantum dots*, Phys. Rev. B **60**, 16611 (1999).

[89] A. Karlhede, S. A. Kivelson, K. Lejnell, and S. L. Sondhi, *Textured Edges in Quantum Hall Systems*, Phys. Rev. Lett. **77**, 2061 (1996).

[90] S.-R. Eric Yang and A. H. MacDonald, *Coupling between edge and bulk in strong-field quantum dots*, Phys. Rev. B **66**, 041304(R) (2002).

[91] T. Chakraborty and P. Pietiläinen, *The Quantum Hall Effects: Fractional and Integral* (Springer, Berlin, 1995).

[92] M. Wagner, U. Merkt, and A. V. Chaplik, *Spin-singlet-spin-triplet oscillations in quantum dots*, Phys. Rev. B **45**, 1951 (1992).

[93] A. Harju, S. Siljamäki, and R. M. Nieminen, *Two-Electron Quantum Dot Molecule: Composite Particles and the Spin Phase Diagram*, Phys. Rev. Lett. **88**, 226804 (2002).

[94] M. A. M. de Aguiar, *Eigenvalues and eigenfunctions of billiards in a constant magnetic field*, Phys. Rev. E **53**, 4555 (1996).

[95] V. Halonen, P. Hyvönen, P. Pietiläinen, and T. Chakraborty, *Effects of scattering centers on the energy spectrum of a quantum dot*, Phys. Rev. B **53**, 6971 (1996).